FRACTURE TOUGHNESS OF ALLOY 690 AND EN52 WELD IN AIR AND WATER

C. M. Brown and W. J. Mills

June 1999

RECEIVED
NOV 22 1999
OSTI

DISCLAIMER

DISCLAIMER

Portions of this document may be illegible in electronic image products. Images are produced from the best available original document.

FRACTURE TOUGHNESS OF ALLOY 690 AND EN52 WELD IN AIR AND WATER

C. M. Brown and W. J. Mills

ABSTRACT

The effect of low and high temperature water with high hydrogen on the fracture toughness of Alloy 690 and its weld, EN52, was characterized using elastic-plastic J_{Ic} methodology. While both materials display excellent fracture resistance in air and elevated temperature (>93°C) water, a dramatic degradation in toughness is observed in 54°C water. The loss of toughness is associated with a hydrogen-induced intergranular cracking mechanism where hydrogen is picked up from the water. Comparison of the cracking behavior in low temperature water with that for hydrogen-precharged specimens tested in air indicates that the critical local hydrogen content required to cause low temperature embrittlement is on the order of 120 to 160 ppm. Loading rate studies show that the cracking resistance is significantly improved at rates above ~1000 MPa√m/h because there is insufficient time to produce grain boundary embrittlement. Electron fractographic examinations were performed to correlate cracking behavior with microstructural features and operative fracture mechanisms.

A690JIC4

INTRODUCTION

Alloy 690 is an attractive candidate for replacing Alloy 600 components in primary water reactor (PWR) applications when stress corrosion cracking (SCC) is a design concern. Indeed, testing to date has shown that this material is immune to high temperature SCC in primary and pure water regardless of microstructure and heat treatment condition.[1-5] The composition of Alloy 690 is similar to that for Alloy 600, except that its chromium content has been doubled from about 15% to 30%. As a result of its superior SCC resistance, Alloy 690 has been used to replace Alloy 600 pressurizer heater sleeves and instrument nozzles, as well as steam generator tubes.[6,7]

Alloy 690 is typically welded using either EN82H or EN52 weld filler metals. EN82H, which is also used to weld Alloy 600 components, is rather susceptible to high temperature SCC. While the SCC resistance for EN52 is far superior to that for EN82H,[1] its inferior weldability has limited its use.

The expected failure mechanisms for welded Alloy 600 and Alloy 690 components involve crack initiation and propagation due to SCC or corrosion fatigue, followed by stable or unstable tearing when a critical crack size is reached. This study focuses on the final step in the cracking process involving stable and unstable fracture. While these materials exhibit excellent toughness in air, fracture properties are degraded in low temperature water.[1] Extensive testing of Alloy 600 and EN82H welds showed that these materials have exceptionally high fracture toughness in air and high temperature water.[8] In low temperature water, Alloy 600 showed a modest decrease in toughness, but retained sufficient cracking resistance to avoid fracture concerns. By contrast, EN82H welds tested in low temperature (<149°C) water exhibited a dramatic reduction in toughness as J_{Ic} and tearing moduli were reduced by one to two orders of magnitude. The reduction in toughness was associated with a hydrogen embrittlement mechanism whereby hydrogen from the water weakened grain boundaries and promoted planar slip, which localized strain concentrations along grain boundaries.

A preliminary study[1] indicated that Alloy 690 and EN52 weld metal also exhibit a significant loss of toughness in low temperature water. Thus, the purpose of this work is to determine the effects of low and high temperature water with high hydrogen on the cracking

resistance of these materials. Fracture properties were determined in 24° to 338°C air and hydrogenated water using elastic-plastic J_{Ic} methodology due to their ductile response. Scanning electron microscopy (SEM) examinations of fracture surfaces were performed to correlate trends in fracture toughness behavior with operative cracking mechanisms. The role of hydrogen embrittlement in degrading fracture properties was evaluated by comparing the cracking behavior in low temperature water with that for hydrogen-precharged specimens tested in low temperature air and water.

MATERIALS AND EXPERIMENTAL PROCEDURE

Test Materials

The Alloy 690 test materials included a 76 mm diameter bar (Heat A) and a 64 mm diameter bar (Heat B). Both heats were tested in the as-received condition, which involved a 1074°C anneal for 5 minutes with an air cool, followed by a 718°C thermal treatment for 10 hours with an air cool. The EN52 welds were fabricated by two manufacturers ["B" and "C"-- vendor identification is consistent with Reference (8)] using a manual gas-tungsten-arc (GTA) weld process. Welds manufactured by Vendor "B" joined Alloy 690 to EN82 clad A516 Grade 60 steel using a 100% argon shield gas. Welds manufactured by Vendor "C" joined two Alloy 690 plates and used either a 100% argon shield gas ("C1") or a 98%/2% argon/hydrogen shield gas ("C2") for improved weldability. All welds were tested in the as-welded condition. Chemical compositions and mechanical properties for the test materials are provided in Tables 1 and 2.

Representative microstructures for the test materials are shown in Figure 1a. The Alloy 690 heats exhibit a uniform grain size with a mean grain diameter of about 75 μm. Grain boundaries are decorated with rather fine chromium-rich $M_{23}C_6$ carbides and there is evidence of ghost boundaries of carbides.

The EN52 welds have well-defined grain boundaries separating colonies of similarly oriented dendrites, as shown in Figure 1b. Grain boundaries are decorated with small titanium-rich MC and chromium-rich $M_{23}C_6$ carbides. Intermediate size carbides are also observed in the interdendritic regions. These interdendritic carbides sometimes pin the grain boundaries.

Fracture Toughness Testing

Fracture tests were performed on precracked compact tension (CT) specimens that had a width (W) of 30.5 mm, a thickness (B) of 15.2 mm and 20% side grooves. The weld specimens were tested in the longitudinal orientation, where the notch was parallel to the welding direction.

Specimens were tested in air and water using servo-electric feedback-controlled systems that were operated in displacement control. Low loading rates, 4 MPa√m/h at 54°C and 0.4 to 2 MPa√m/h at 338°C, were used to allow sufficient time for environmental effects to occur. Loading rates for a few 54°C water tests were also varied betweeen 0.4 and 26,000 MPa√m/h to evaluate rates effects on environmental cracking behavior.

In accordance with multiple-specimen J_{IC} test procedures, specimens were unloaded when the target displacement was reached, heat tinted to discolor the crack extension region, and subsequently fatigued apart so the amount of crack extension (Δa) could be measured by the ASTM E1737-96 nine-point measurement method. Because external load cells were used to measure test load in autoclave tests, the seal friction load was measured and subtracted from the load measurement at the beginning of the test. Load-line displacement values for each specimen were computed from external LVDT displacement measurements using the correction procedures outlined in Reference (8) to subtract out extraneous load-train displacements. The corrected load versus load-line displacement data were used to compute J in accordance with ASTM E1737-96.

The multispecimen J-R curve method was used to establish J_{IC} values, because the periodic unload/reload cycles associated with the unloading compliance method could possibly affect the environmental cracking behavior in water. The overall J_{IC} analysis methods were patterned after ASTM E1737-96. J-R curves were constructed by plotting J values against the corresponding crack extension values (Δa) and fitting the J-Δa data with a power-law regression line. The J_{IC} toughness was the value of J at the intersection of the power-law curve with the 0.2 mm offset blunting line:

$$\Delta a = \frac{J}{4\sigma_f} + 0.2 \ (mm) \tag{1}$$

where σ_f is the flow strength, which is equal to the average of the yield and ultimate strength levels [i.e., $\sigma_f = (\sigma_{YS} + \sigma_{UTS})/2$]. Note that the blunting line developed for high strain hardening materials,[9] $J = 4\sigma_f (\Delta a)$, accurately estimates the apparent blunting behavior for both the wrought and weld metals. Values of the tearing modulus (T), which represents a dimensionless measure of the tearing resistance after J_{IC} is exceeded, were calculated from the following equation:[10]

$$T = \frac{dJ}{da} \frac{E}{\sigma_f^2} \qquad (2)$$

where dJ/da is the average slope of the J-R curve (at $\Delta a \approx 1.3$ mm) and E is the elastic modulus. For specimens that exhibited relatively little plasticity prior to the onset of environmental cracking, equivalent critical stress intensity factors (K_{JC}) were computed from experimental J_{IC} values using the equation[11]

$$K_{JC} = \sqrt{E J_{IC}} \qquad (3)$$

Although the number and spacing of J-Δa data points do not always conform to ASTM guidelines, the J_{IC} values obtained herein are judged to be accurate estimates of the materials fracture toughness. In cases where insufficient data preclude multiple-specimen J_{IC} analysis, a modified version of the normalization technique proposed by ASTM Task Group E08.08.02 was used to determine J_{IC} and T. A detailed description of the normalization method is provided in Reference (12). In this paper, multispecimen and normalized J-R curves are represented by solid and broken lines, respectively.

<u>Test Environment</u>

Flowing autoclaves were used to conduct tests in hydrogenated deaerated water at 24°, 54°, 93°, 149° and 338°C. Room temperature pH was 10.1 to 10.3 and the oxygen concentration typically ranged between 3 and 17 ppb. The nominal hydrogen concentration was 150 cc H_2/kg H_2O, but ranged from 140 to 180 cc H_2/kg H_2O.

<u>Hydrogen Precharging</u>

Hydrogen precharging was conducted in a high pressure autoclave using 99.999% pure hydrogen. As-fabricated CT specimens were first cleaned in acetone and then rinsed in alcohol before being inserted into the autoclave. To assure a uniform hydrogen distribution, precharging runs were performed at 360°C for 6 weeks. After precharging, the specimens were refrigerated below 0°C to minimize hydrogen loss. Hydrogen concentrations for at least two specimens for each test material were measured after rising load testing was complete. Chips produced by hole drilling were collected for hydrogen analysis. Care was taken not to

heat the sample or contaminate the chips. Vacuum extraction analysis on a LECO hydrogen analyzer was performed to measure hydrogen content. The range of hydrogen concentrations was 64 to 67 ppm for Alloy 690 and 68 to 77 ppm for EN52 weld.

Fracture Toughness Testing of Hydrogen-Precharged Specimens

Hydrogen-precharged CT specimens were also tested in 24°C air and hydrogenated water at a nominal $\dot{K}$ of 3 MPa√m/h. The resulting load versus load-line displacement curves and maximum stress intensity factors (K_{Pmax}) were compared with those obtained for non-precharged specimens tested in water to determine if hydrogen embrittlement is responsible for the degraded fracture toughness response in low temperature water. Values of K_{Pmax} were computed by substituting the maximum load and initial crack length into the K solution in ASTM E1737-96. While K_{Pmax} values are not strictly valid when significant plasticity occurs (i.e., >60 MPa√m), they provide a relative ranking of susceptiblity to low temperature cracking.

Fractographic Examinations

Broken specimen halves were examined on an SEM to characterize the fracture surface morphology in order to compare operative cracking mechanisms for hydrogen-precharged and non-precharged specimens.

RESULTS AND DISCUSSION

Fracture of Alloy 690

The cracking behavior for the two Alloy 690 heats in air and water is summarized in Figures 2 and 3. It is seen that the fracture response for Heat A in air is independent of temperature, so the 24°-54° and 338°C data were combined into a single J-R curve yielding a J_{IC} of 447 kJ/m² and T of 448. High temperature water has almost no effect on toughness as J_{IC} and T values are within 10% of their air counterparts. While the fracture toughness of Heat B in 338°C water (J_{IC} of 358 and T of 242) is slightly less that that for Heat A, it still possesses excellent fracture resistance. In summary, the exceptionally high toughness values in air and high temperature water demonstrate that fracture is not an issue for Alloy 690 components under these conditions.

In 54°C water, there is a substantial reduction in toughness as J_{IC} values drop to 69 and 20 kJ/m² and T drops to 38 and 24. Although the J_{IC} values are low, Alloy 690 exhibits some plastic deformation prior to the onset of environmental cracking and the tearing moduli indicate that modest tearing resistance is retained. Based on these findings, low temperature crack propagation (LTCP) is not viewed as a primary engineering concern for Alloy 690. However, for critical components where the consequences of failure are a concern, fracture mechanics assessments should be performed to guard against fracture.

The cracking resistance is significantly increased when the water temperature is increased to 93°C (Figure 3) and it is fully restored at 149°C (Figures 2 and 3). Therefore, LTCP in Alloy 690 is an issue only at temperatures below 93°C.

Figure 4, which summarizes displacement rate effects on LTCP behavior, shows that LTCP susceptibility is essentially rate independent below 15 mm/h ($\dot{K} \leq 1300$ MPa√m/h). Within this domain, longer exposure times do not further embrittle the crack tip region. Increasing the rate to 305 mm/h (26,000 MPa√m/h) is seen to fully restore cracking resistance. At this rate there is insufficient time to embrittle the crack tip region. Therefore, transient loading events with $\dot{K}$ greater than about 25,000 MPa√m/h will not cause environmental cracking in low temperature water.

The Alloy 690 fracture surfaces generated in air and 338°C water were found to be indistinguishable, as shown in Figure 5. This is consistent with the lack of an effect of elevated temperature air or water on the toughness response. Fracture surfaces are comprised of large primary dimples nucleated by broken MC carbide inclusions, smaller dimples nucleated by ghost boundary carbides and shear-stretch regions.[8] The shear-stretch morphology, which covers a large portion of the fracture surface, is characterized by a rather nondescript appearance with evidence of wavy slip lines normal to the crack growth direction and a few elongated (shear) dimples. This mechanism is associated with an alternating shear rupture process[13] that operates when very high shear stresses develop in the ligaments between primary microvoids. The observation of well-defined dimples and serpentine slip on dimple walls and in shear-stretch regions indicates that the fracture process involves extensive plastic deformation, which accounts for the high toughness observed in air and 338°C water.

In 54°C water, intergranular cracking is dominant (Figures 6a and 6b). There is also limited evidence of transgranular cracked regions with poorly defined facets (Figure 6c), but no evidence of dimple rupture or shear-stretch regions. High magnification of grain boundaries revealed a rough appearance, as shown in Figure 6b. There appears to be two causes of this rough texture: in some regions an outline of the intergranular $M_{23}C_6$ carbides produces the jagged structure, while in other regions the rough appearance suggests that the crack is actually propagating in the matrix immediately adjacent to grain boundaries. The intergranular cracking and transgranular faceting are believed to result from a hydrogen embrittlement mechanism, as discussed later.

Fracture of EN52 Welds

Figure 7 shows that EN52 weld metal exhibits exceptionally high toughness in air and high temperature water. The cracking response in air is independent of temperature, so the 54° and 338°C data were pooled to establish a common J-R curve that yielded a J_{Ic} of 814 kJ/m² and T of 484. High temperature water is seen to have essentially no effect on toughness, as J_{Ic} is 1060 kJ/m² and T is 540. These incredibly high toughness values demonstrate that fracture is not a design or operation concern for EN52 welds in air and high temperature water.

8

In 54°C water, however, there is a dramatic reduction in toughness, as illustrated in Figures 7 and 8. For Weld "B1-b", J_{IC} decreases to 37-47 kJ/m² and T decreases to 31-48. For Welds "C1" and "C2", J_{IC} is 27 kJ/m² and T is only 4. These low toughness values suggest that LTCP is a concern for highly loaded EN52 welds.

Because low temperature cracking in the more embrittled welds (i.e., Welds "C1" and "C2") typically initiates prior to the onset of significant plastic deformation, it is not surprising that K_{Pmax} values, which range from 53 to 83 MPa√m, are in reasonable agreeement with the K_{JC} value of 74 MPa√m, which is computed from the experimental J_{IC} value of 27 kJ/m². This agreement suggests that LTCP in the most embrittled welds tends to initiate at or slightly before maximum load within the linear-elastic domain. Therefore, the lower-bound K_{Pmax} of 53 MPa√m can be used in linear-elastic fracture mechanics assessments to estimate the limiting response.

Although EN52 weld shows a severe toughness degradation in 54°C, its fracture resistance is considerably greater than that for EN82H welds. Lower-bound J_{IC} and K_{Pmax} values for EN82H welds[8] with the same crack orientation are 14 kJ/m² and 40 MPa√m, respectively.

It is noted that one of the welds manufactured by Vendor "B" exhibited tremendous variability in LTCP behavior. Figure 7 shows that low temperature water has no effect on the toughness response for two specimens from Weld "B1-a", a slight effect for a third specimen and a substantial effect for the fourth. In contrast with this behavior, all three specimens machined from Weld "B1-b", which was fabricated by the same vendor using the same materials and welding parameters, were very susceptible to LTCP in 54°C water. The reason for this variability is unknown.

Increasing the water temperature to 93° and 149°C significantly increases the weld's cracking resistance, as shown in Figure 8. The high J_{IC} values, 218 kJ/m² at 93°C and 453-594 kJ/m² at 149°C, coupled with tearing moduli above 300 demonstrate that LTCP is not a concern at and above 93°C.

Figure 9, which presents displacement rate effects on LTCP behavior, shows that the cracking response at 0.05 and 0.005 mm/h ($\dot{K}$ = 4 and 0.4 MPa√m/h) are the same, thereby indicating that longer exposure times do not cause additional embrittlement. Increasing the rate

9

to 15 mm/h (1300 MPa√m/h) causes a modest increase in cracking resistance, $J_{IC} = 133$ kJ/m²
and $T = 70$, and at 305 mm/h (26,000 MPa√m/h) there is a significant increase in toughness,
$J_{IC} = 395$ kJ/m² and $T = 434$. At the higher rates, there is insufficient time to embrittle the
crack tip region. Therefore, transient loading events with $\dot{K}$ greater than ~1000 MPa√m/h will
not cause severe embrittlement.

The fracture surface topography for EN52 welds tested in air and 338°C water consists
of dimples and shear-stretch markings, as shown in Figure 10. Extensive evidence of
serpentine slip offsets on the fracture surface indicates that tremendous amounts of platic
deformation are required to propagate the crack. This is consistent with the exceptionally high
J_{IC} values observed under these test conditions.

The reason why the weld exhibits greater cracking resistance than wrought Alloy 690
is the lack of large primary MC inclusions in the former. In the wrought material, the coarse
inclusions fracture and nucleate large microvoids at plastic strains of just a few percent. The
absence of coarse inclusions in the weld suppresses microvoid nucleation. Additional plastic
energy is needed for microvoid nucleation because the smaller carbides resist fracture.
Eventually, the intermediate size interdendritic carbides fail by a decohesion process, but at
much greater strains.

In 54°C water, a fracture morphology transition from ductile tearing to intergranular
cracking is responsible for the dramatic degradation in cracking resistance. The intergranular
surfaces have a rather smooth and undulating appearance (Figure 11a) that reflects the
dendritic morphology of the weld. At high magnification, grain boundaries are seen to be rather
featureless (Figure 11b). Isolated islands containing transgranular facets are also observed, as
shown at the bottom of Figure 11a. The facets tend to be steeply inclined to the overall
fracture surface as they link two adjacent intergranular cracks at different elevations. This
morphology indicates that unbroken ligaments are left in the wake of advancing intergranular
cracks because grain boundaries in these regions resisted cracking. After the primary crack
extends well beyond these ligaments, the local stresses are large enough to nucleate
transgranular faceting. Macroscopic examination of fracture surfaces provides additional
support for this cracking mechanism. Bright (non-heat tinted) ligaments are found within the
LTCP (i.e., heat tinted) region, just behind the final crack front. This indicates that grain

boundaries within these regions did not fail and local stresses were too low to induce crystallographic faceting.

Low Temperature Cracking Mechanism

The nature of low temperature cracking in Alloy 690 and EN52 is very similar to that observed in EN82H welds, which was shown to be associated with a hydrogen-embrittlement mechanism. To evaluate the role of hydrogen in embrittling Alloy 690 and EN52 welds, CT specimens precharged with 64-77 ppm hydrogen were tested in air in an attempt to reproduce the degree of embrittlement and cracking mechanisms found in low temperature water. Most tests were conducted at a $\dot{K}$ of 4 MPa$\sqrt{m}$/h so there would be sufficient time to fully embrittle the crack tip region. A few hydrogen precharged specimens were also tested at 4×10^5 MPa$\sqrt{m}$/h (1-3 seconds to reach maximum load) to preclude hydrogen from diffusing and accumulating ahead of a crack. These tests are designed to help define the minimum lattice hydrogen content required to cause low temperature embrittlement. Hydrogen-precharged specimens were also tested in 54°C water to determine if hydrogen from the water combines with hydrogen already present to cause additional embrittlement.

Figure 12 compares K_{Pmax} for hydrogen-precharged and non-precharged specimens tested in air and low temperature water. For EN52, K_{Pmax} for the precharged specimen tested in air, 68 MPa$\sqrt{m}$, agrees with the range of values, 68-74 MPa$\sqrt{m}$, observed for non-precharged specimens tested in 54°C water. A similar trend is observed for Alloy 690, whereby K_{Pmax} for the precharged specimen tested in air, 53 MPa$\sqrt{m}$, is within the range of values, 46-68 MPa$\sqrt{m}$, for non-precharged specimens tested in 54°C water. Moreover, load-displacement curves for the hydrogen-precharged specimens tested in air and non-precharged specimens tested in 54°C water were similar, indicating that the degree of embrittlement in low temperature water is reproduced by hydrogen-precharging.

Fractographic examinations show that cracking mechanisms operative in low temperature water are reproduced by testing precharged specimens in air. Figure 13 shows the intergranular cracking with a rough texture and transgranular faceting in precharged Alloy 690 that is reminiscent of the fracture surface appearance associated with LTCP in water (Figure 6). The only notable difference in fracture surface morphology is somewhat better defined crystallographic facets for the precharged specimens. In some regions facets have a very

11

crystallographic appearance, as shown in Figure 13b, indicative of a channel fracture mechanism where localized separation occurs along intense planar slip bands.[14,15] The presence of channel fracture in precharged specimens provides strong evidence that hydrogen promotes heterogeneous slip and lowers the cohesive strength between atoms thereby causing local separation along planar slip bands. A decohesion mechanism whereby hydrogen decreases cohesive strength and promotes failure along specific crystallographic planes was originally proposed by Steigerwald et al.[16]

The fracture surface appearance for hydrogen-precharged EN52 tested in air is identical to that for the non-precharged weld tested in 54°C water. Intergranular cracking is the dominant mechanism (Figure 14) and there is limited evidence of transgranular facets. Once again, the transgranular regions are steeply inclined to the overall fracture plane demonstrating that they are associated with the high shear stresses that develop in unbroken ligaments left in the wake of the advancing intergranular crack.

The observation that hydrogen-precharged specimens tested in air reproduce the degree of embrittlement and cracking mechanisms observed in low temperature water demonstrates that LTCP involves a hydrogen embrittlement mechanism. Hydrogen appears to play a dual role as it reduces the grain boundary cohesive strength and promotes planar slip which enhances strain concentrations along grain boundaries. Hydrogen also induces transgranular faceting; however, this mechanism is judged to be less important because it occurs very late in the cracking process as the large intergranular cracks coalesce.

Figure 12 also shows that testing hydrogen-precharged specimens in water produces the most severe embrittlement. This indicates that hydrogen from the water further increases the hydrogen content ahead of a crack, which further degrades toughness. Apparently, hydrogen from the water is added to the precharged hydrogen to severely weaken grain boundaries, fill traps and promote planar slip. It is also noted that the presence of hydrogen in the water minimizes the loss of precharged hydrogen from the crack tip region. The fracture surface morphologies for the precharged specimens tested in water (Figure 13c and Figure 14b) are virtually identical to their air counterparts (Figure 13a and 14a).

Rapid loading of precharged Alloy 690 fully restores K_{Pmax} (Figure 12). Comparison of load-displacement records indicates that the ability to plastically deform is restored as well. The

fracture surface is predominantly transgranular, consisting of shear-stretch markings and dimples. Dimple growth is stunted, however, by the onset of a faceting mechanism. Intergranular fracture is also observed, but confined to a few isolated regions.

Rapid loading of hydrogen-precharged EN52 restores K_{Pmax} to 100 MPa√m, but comparison of load-displacement records shows that the amount of plastic deformation is less than that for non-precharged specimens tested in air. Under rapid loading conditions, the fracture surface is predominantly transgranular, consisting of dimples and poorly defined facets, with a few isolated patches of intergranular cracking. Two types of slip offsets are observed: wavy offsets are superimposed on dimple walls and planar offsets are sometimes found on steeply inclined facets. Finding both wavy and planar slip offsets under rapid loading conditions, whereby hydrogen cannot diffuse, indicates that a hydrogen content of about 70 ppm is the critical amount to initiate a transition from homogeneous to heterogeneous slip.

The high K_{Pmax} values observed under rapid loading conditions indicate that 65 ppm hydrogen in Alloy 690 and 70 ppm hydrogen in EN52 is insufficient to severely embrittle these materials, but these levels produce the first signs of intergranular cracking and crystallographic faceting. Apparently, higher local hydrogen concentrations are developed within the crack tip region in slowly loaded specimens.

The critical local hydrogen concentrations required for LTCP can be estimated from the slow test of the precharged specimens by assuming that there is sufficient time for hydrogen to diffuse and accumulate ahead of the crack. Under equilibrium conditions, local hydrogen concentrations are estimated using the relationship:[17]

$$\frac{C}{C_o} = \exp\frac{\sigma_H \overline{V}}{RT} \tag{4}$$

where:

C = local hydrogen concentration
C_o = bulk hydrogen concentration
σ_H = hydrostatic stress
$\overline{V}$ = partial molar volume of hydrogen in solid solution
R = universal gas constant
T = absolute temperature

$\overline{V}$, defined as the change in volume produced by the addition of 1 gram-mol of hydrogen into a metal, is estimated to be 1.8 cm^3/mol based on lattice parameter measurements for solutions of hydrogen in nickel and other face-centered cubic metals.[18,19] The peak hydrostatic stress is estimated from References (20) and (21), which reported that the peak stress ahead of a crack in high strain hardening materials is about five times the yield strength. Assuming plane strain conditions, the peak hydrostatic stress is about 50% of the peak normal stress or 2.5 times the yield strength.

Based on Equation (4), the peak C/Co ratios at 24°C are 1.8 for Alloy 690 (σ_{ys} = 345 MPa) and 2.2 for EN52 (σ_{ys} = 415 MPa). Therefore, peak hydrogen concentrations for the precharged specimens that were slowly loaded in air were calculated to be ~120 ppm for Alloy 690 and ~160 ppm for EN52. Because these specimens showed essentially the same degree of embrittlement as that observed for non-precharged specimens tested in 54°C water, critical lattice hydrogen concentrations to produce LTCP are estimated to be in the range of 120 to 160 ppm. This assumes that cracking events nucleate near the peak triaxial stress location.

In summary, local hydrogen concentrations of about 70 ppm induce the first signs of intergranular cracking, but are insufficient to cause significant embrittlement. Full grain embrittlement occurs at approximately 120 to 160 ppm, which agrees with EN82H weld findings where the critical hydrogen content to cause LTCP was estimated to be 130 ppm.[8] It is noted that hydrogen concentrations at grain boundaries are actually higher than those levels for the surrounding lattice because grain boundaries and grain boundary carbides serve as effective hydrogen traps.

CONCLUSIONS

The fracture toughness of Alloy 690 and EN52 welds was characterized in 24° to 338°C air and water with 150 cc H_2/kg H_2O. The results of this work are provided below.

1. The excellent fracture toughness displayed by Alloy 690 and EN52 in air and elevated temperature water demonstrates that fracture is not an issue under these conditions.

2. The fracture resistance of both materials is dramatically reduced in 54°C water, as J_{IC} and tearing moduli are reduced by one to two orders of magnitude. Low temperature fracture is not viewed as a primary engineering concern for Alloy 690 because some plastic deformation precedes cracking and a modest tearing resistance is retained. Some welds show little or no plasticity prior to cracking and tearing moduli as low as 4, so fracture is a potential concern in low temperature water.

3. Because LTCP in the most embrittled welds initiates within the linear-elastic domain, the lower-bound K_{Pmax} of 53 MPa$\sqrt{m}$ can be used in fracture mechanics evaluations to assess structural integrity of welded components.

4. Increasing the water temperature to 93°C and above significantly improves cracking resistance in both Alloy 690 and EN52; hence, LTCP is not a concern above this temperature.

5. Low temperature cracking is not an issue for short-term transients where loading rates exceed 25,000 MPa$\sqrt{m}$/h because there is insufficient time for embrittlement to occur. For EN52 weld, a modest increase in cracking resistance is observed at 1300 MPa$\sqrt{m}$/h.

6. The toughness degradation displayed by Alloy 690 and EN52 in 54°C water is attributed to a hydrogen-induced intergranular cracking mechanism. Hydrogen from the water reduces grain boundary cohesive strength and promotes planar slip which localizes strain concentrations along grain boundaries. Results from hydrogen-precharged specimens indicate that the critical hydrogen content in the lattice to produce LTCP is on the order of 120 to 160 ppm.

15

ACKNOWLEDGEMENT

REFERENCES

(1)   C. M. Brown and W. J. Mills, "Effect of Water on Mechanical Properties and Stress Corrosion Behavior of Alloy 600, Alloy 690, EN82H Welds and EN52 Welds," Corrosion, 1999, in press.

(2)   K. Norring, J. Engstrom and P. Norberg, "Intergranular Stress Corrosion Cracking in Steam Generator Tubing, Testing of Alloy 690 and Alloy 600 Tubes," Proceedings of the Third International Symposium on Environmental Degradation of Materials in Nuclear Power Systems--Water Reactors, TMS, 1988, pp. 587-593.

(3)   R. G. Aspden, T. F. Grand and D. L. Harrod, "Corrosion Performance of Alloy 690," Proceedings: 1989 EPRI Alloy 690 Workshop, EPRI Report NP-6750-SD, April 1990.

(4)   R. A. Page, "Stress Corrosion Cracking of Alloys 600 and 690 and Nos. 82 and 182 Weld Metals in High Temperature Water," Corrosion, Vol. 39, 1983, pp. 409-421.

(5)   T. Yonezawa, K. Onimura, N. Sasaguri, T. Kusakabe, H. Nagano, K. Yamanaka, T. Minami and M. Inoue, "Effect of Heat Treatment on Corrosion Resistance of Alloy 690," Proceedings of the Second International Symposium on Environmental Degradation of Materials in Nuclear Power Systems--Water Reactors, ANS, 1986, pp. 593-600.

(6)   P. Saint Paul and G. Slama, "Steam Generator Materials Degradation," Proceedings of the Fifth International Symposium on Environmental Degradation of Materials in Nuclear Power Systems--Water Reactors, ANS, 1992, pp. 39-49.

(7)   A. S. O'Neill and J. F. Hall, "Literature Survey of Cracking of Alloy 600 Penetrations in PWR's," EPRI Report NP-7094, December 1990.

(8)   C. M. Brown and W. J. Mills, "Fracture Toughness of Alloy 600 and EN82H Welds in Air and Water," B-T-3264, 1999.

17

(9)   W. J. Mills, "On the Relationship Between Stretch Zone Formation and the J Integral for High Strain-Hardening Materials," Journal of Testing and Evaluation, Vol. 9, 1981, pp. 56-62.

(10) P. C. Paris, H. Tada, A. Zahoor and H. Ernst, "The Theory of Instability of the Tearing Mode for Elastic-Plastic Crack Growth," Elastic-Plastic Fracture, ASTM STP 668, 1979, pp. 5-36.

(11) J. A. Begley and J. D. Landes, "The J Integral as a Fracture Criterion," Fracture Toughness, Proceedings of the 1971 National Symposium on Fracture Mechanics, Part II, ASTM STP 514, 1972, pp. 1-20.

(12) W. C. Porr and W. J. Mills, "Application of the Normalization Data Analysis Technique for Single Specimen R-Curve Determination," Bettis Atomic Power Laboratory, Report, B-T-3269, February 1999.

(13) R. M. N. Pelloux, "Crack Extension by Alternating Shear," Engineering Fracture Mechanics, Vol. 1, 1970, pp. 697-704.

(14) C. W. Hunter, R. L. Fish and J. J. Holmes, "Channel Fracture in Irradiated EBR-II Type 304 Stainlesss Steel," Transactions of the American Nuclear Society, Vol. 15, 1972, pp. 254-255.

(!5) W. J. Mills, "The Deformation and Fracture Characteristics of Inconel X-750 at Room Temperature and Elevated Temperatures," Metallurgical Transactions, Vol. 11A, 1980, pp. 1039-1047.

(16) E. A. Steigerwald, F. W. Schaller and A. R. Troiano, "The Role of Stress in Hydrogen Induced Delayed Failure," Transactions of the AIME, Vol. 218, 1960, pp. 832-841

(17) W. W. Gerberich and Y. T. Chen, "Hydrogen-Controlled Cracking--An Approach to Threshold Stress Intensity," Metallurgical Transactions, Vol. 6A, 1975, pp. 271-278.

(18) B. B. Baranowski, S. Majchrzak and T. B. Flanagan, "The Volume Increase of FCC Metals and Alloys Due to Interstitial Hydrogen Over a Wide Range of Hydrogen Contents," Journal of Physics F: Metal Physics, Vol. 1, 1971, pp. 258-261.

(19) M. L. Wayman and G. C. Smith, "Hydride Formation in Nickel-Iron Alloys," The Journal of Physics and Chemistry of Solids, Vol. 32, 1971, p. 103.

(20) J. R. Rice and M. A. Johnson, "The Role of Large Crack Tip Geometry Changes in Plane Strain Fracture," Inelastic Behavior of Solids, McGraw-Hill, NY, 1970, pp. 641-672.

(21) R. M. McMeeking, "Finite Deformation Analysis of Crack-Tip Opening in Elastic-Plastic Materials and Implications for Fracture," Journal of the Mechanics and Physics of Solids, Vol. 25, 1977, pp. 357-381.

Table 1 - Material Chemistries (weight percent)					
Material	Alloy 690		EN52 Welds		
Heat or Weld	"A" 9486-3	"B" 9518-1	"B1" Y9378K	"C1" Y9378K	"C2" Y9378K
Shield Gas			Ar	Ar	Ar-2% H_2
Element					
C	0.028	0.031	0.035	0.030	0.030
Mn	0.31	0.05	0.26	0.25	0.25
Fe	8.13	8.89	9.7	9.77	9.94
S	<0.001	<0.001	0.001	<0.001	0.001
Si	0.032	0.032	0.28	0.17	0.21
Cu	0.017	0.016	0.003	0.004	0.002
Ni	61.28	60.61	58.55	58.96	58.8
Cr	29.48	29.63	29.5	28.96	28.89
Al	0.36	0.35	0.66	0.66	0.66
Ti	0.32	0.34	0.56	0.50	0.55
P	<0.002	0.002	<0.001	<0.001	<0.001
Nb + Ta	0.003	0.002	0.004	<0.001	0.002

Chem4.wpd

			EN52				Alloy 690			
T	Env	Prop	$\bar{x}$	H	L	s	$\bar{x}$	H	L	s
338°C	Water	σ_{YS} (MPa)	334	411	196	61	281	353	194	70
		σ_{UTS} (MPa)	477	538	347	59	580	625	541	36
		%ϵ	35.7	52.2	18.0	9.4	48.0	62.3	35.7	8.9
		%RA	55.5	70.5	36.5	11.8	56.3	61.2	44.2	6.1
54°C	Water	σ_{YS} (MPa)	414	463	308	48	255	268	234	14
		σ_{UTS} (MPa)	514	573	405	50	553	608	458	67
		%ϵ	32.2	38.2	23.0	4.6	39.9	47.1	16.7	13.1
		%RA	58.5	67.8	48.0	5.8	52.6	64.5	24.1	16.3
338°C	Air	σ_{YS} (MPa)	380	408	352	21	286	343	243	42
		σ_{UTS} (MPa)	522	558	497	19	589	605	556	19
		%ϵ	41.6	56.1	35.8	6.7	49.8	53.8	41.9	4.8
		%RA	57.6	64.4	44.6	7.1	63.4	64.8	61.5	1.2
54°C	Air	σ_{YS} (MPa)	441	483	418	23	311	407	266	59
		σ_{UTS} (MPa)	588	632	527	34	631	647	603	21
		%ϵ	38.6	52.5	27.1	7.1	46.6	51.5	38.9	4.8
		%RA	57.9	67.1	46.1	6.9	63.3	65.9	60.1	2.1
RT	Air	σ_{YS} (MPa)	454	492	395	37	321	393	279	46
		σ_{UTS} (MPa)	635	659	602	21	686	702	677	10
		%ϵ	45.1	59.7	34.4	10.4	56.3	60.9	52.6	3.4
		%RA	63.1	68.1	51.4	6.8	67.7	68.3	67.1	0.5

Table 2 - Summary of Tensile Test Results

T - test temperature, ENV - test environment,
PROP - material properties: σ_{YS} - yield strength, σ_{UTS} - ultimate strength, %ϵ - percent elongation, %RA - percent reduction in area
$\bar{x}$ - average of all data, H - highest data point, L - lowest data point, s - standard deviation of data

FIGURE CAPTIONS

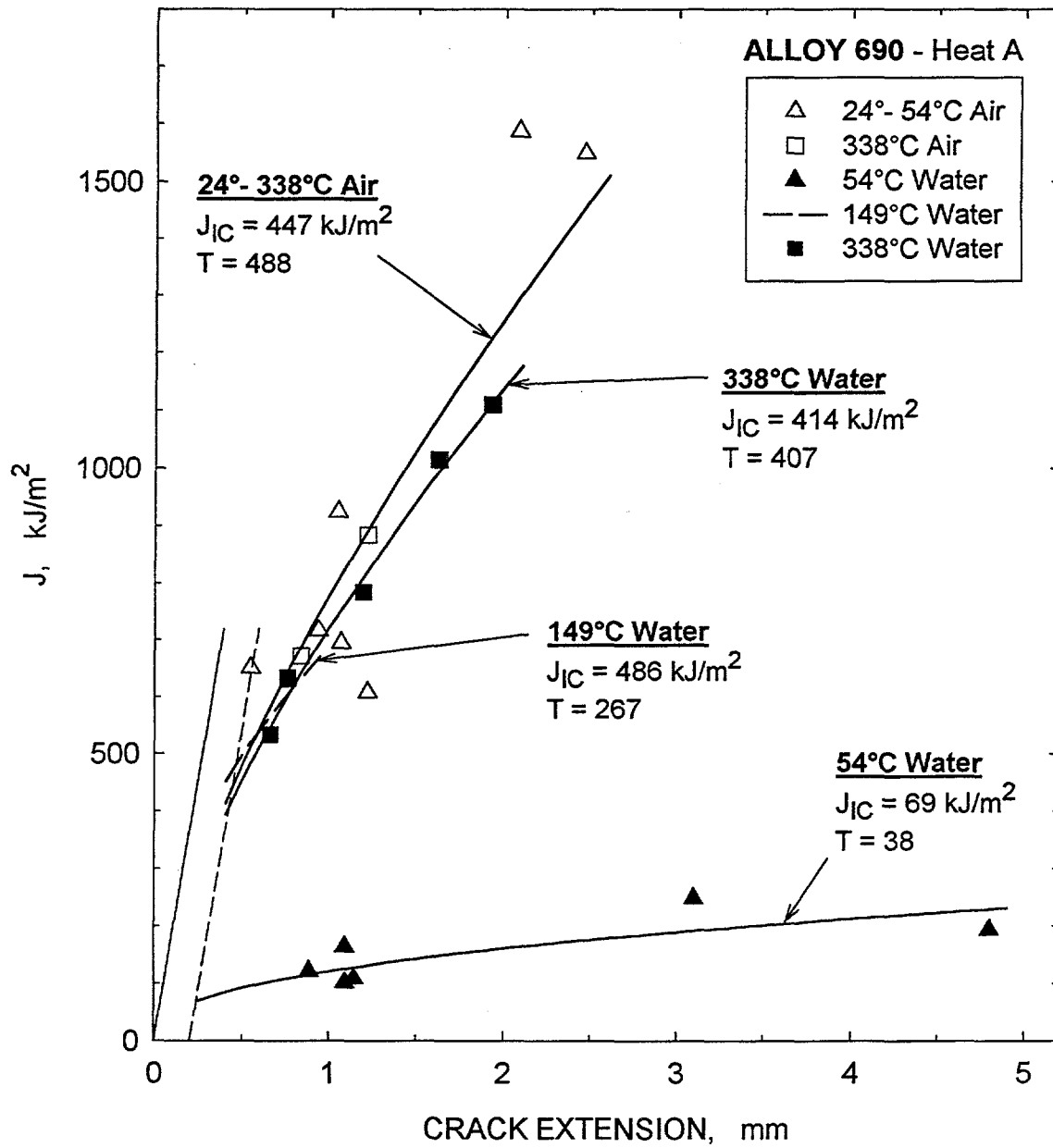Figure 1. Representative microstructures for (a) Alloy 690 and (b) EN52 weld.
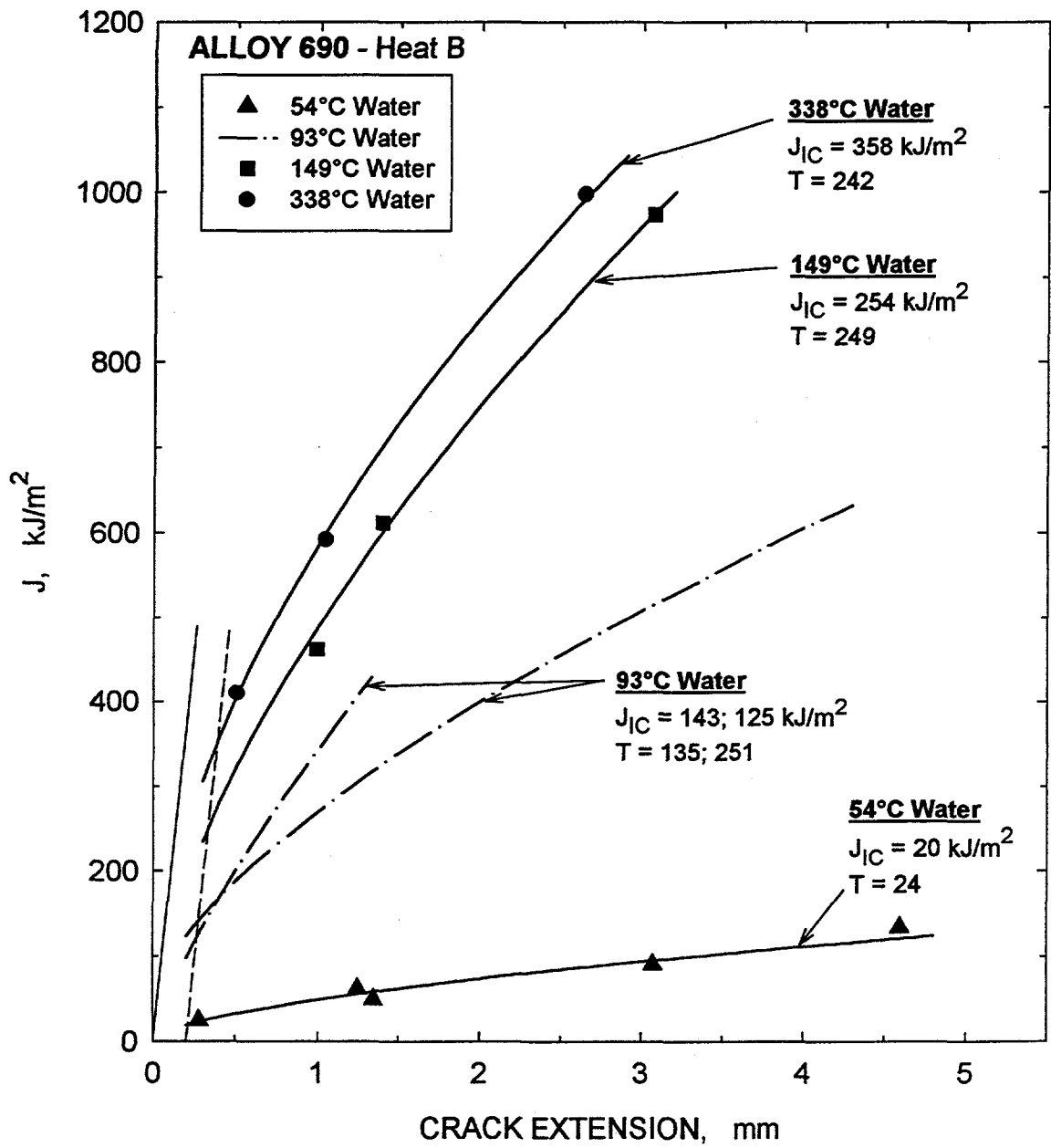
Figure 2. J-R curves for Alloy 690 Heat A in air and water.

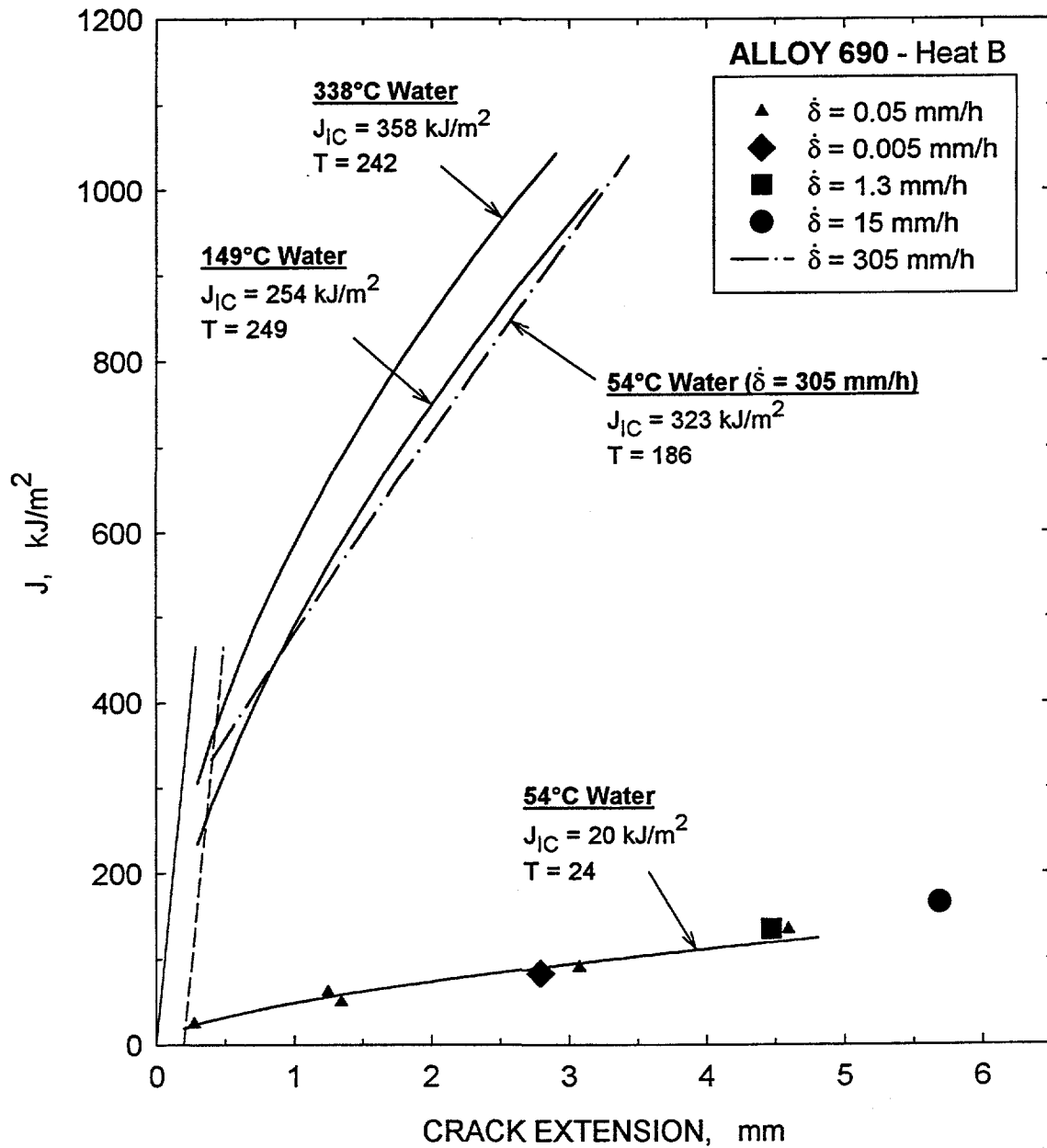Figure 3. J-R curves for Alloy 690 Heat B in water.

Figure 4. Effect of displacement rate on the cracking behavior of Alloy 690 Heat B in water.

Figure 5. Fracture surface features for Alloy 690 tested in air and 338°C water were indistinguishable. (a) 338°C air. Duplex dimple morphology with large dimples nucleated by large carbide inclusions and smaller dimples nucleated by ghost boundary carbides. Note evidence of serpentine slip offsets and elongated shear dimples in the shear-stretch region (on right side). (b) 338°C water. Large and small dimples. (c) 338°C water. Typical shear-stretch region.

Figure 6. SEM fractographs of Alloy 690 tested in 54°C water showing intergranular cracking but no evidence of dimple rupture. (a) Intergranular cracking and poorly defined transgranular facets. (b) High magnification of upper right corner of (a) showing rough appearance of grain boundary walls. (c) Poorly defined transgranular facets.

Figure 7. J-R curves for EN52 weld 'B1' in air and water.

Figure 8. J-R curves for EN52 welds 'C1' and 'C2' in water.

Figure 9. Effect of displacement rate on the cracking behavior of EN52 welds 'C1' and 'C2'.

Figure 10. Fracture surface features for EN52 welds tested in air and 338°C water were indistinguishable. (a) 54°C air. Dimples and shear-stretch region (upper right). (b) 338°C water. Dimples (left) and shear-stretch region (right).

Figure 11. SEM fractographs of EN52 welds tested in 54°C water. (a) Dominant intergranular cracking morphology surrounding island of transgranular faceting (bottom center). (b) Intergranular fracture surfaces were rather featureless.

Figure 12. K_{Pmax} values for EN52 weld and Alloy 690. Non-precharged specimens were tested in 54°C air or water; hydrogen-precharged [H] specimens were tested in 24°C air or water. The short test times for the rapid loading tests [Rap], where maximum load was reached in 1 to 3 seconds, preclude hydrogen from diffusing to the crack tip. Crosshatching represents a range of K_{Pmax} values.

Figure 13. Fracture surface morphology for hydrogen-precharged Alloy 690. (a) Tested in air. Intergranular cracking and transgranular faceting. (b) Tested in air. Crystallographic facets steeply inclined to fracture surface. (c) Tested in water. Intergranular cracking and transgranular faceting.

Figure 14. Fracture surface morphology for hydrogen-precharged EN52 welds. (a) Tested in air. Extensive intergranular cracking with small transgranular islands. (b) Tested in water. Fracture surface is predominantly intergranular.
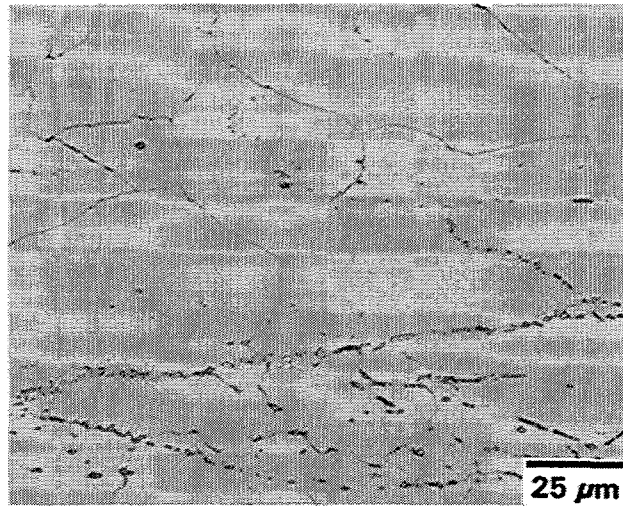
(a)
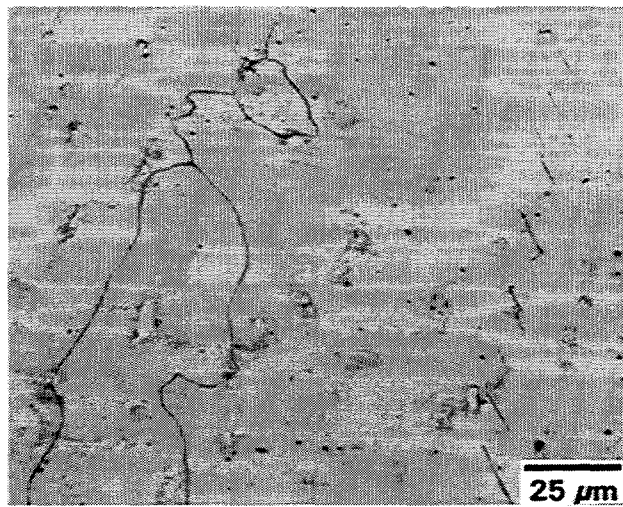
(b)

Figure 1.   Representative microstructures for (a) Alloy 690 and (b) EN52 weld.

Figure 2.   J-R curves for Alloy 690 Heat A in air and water.

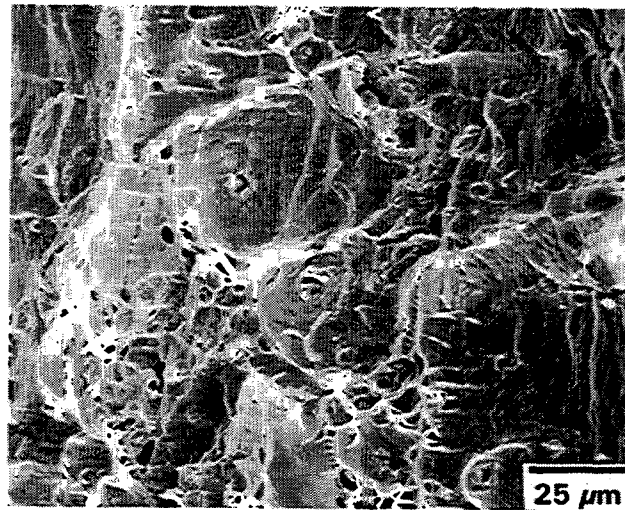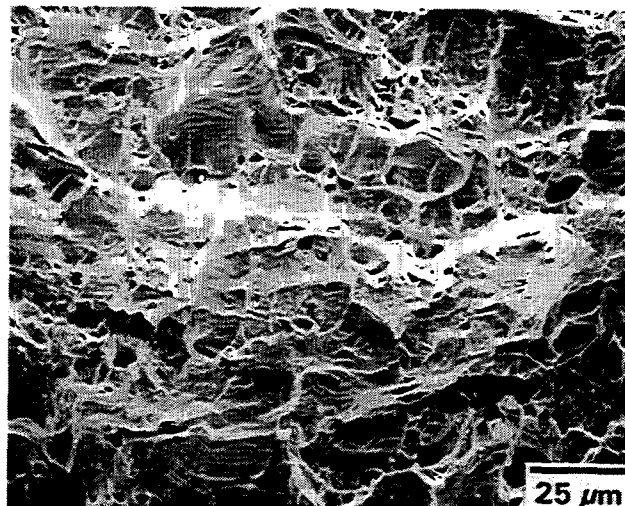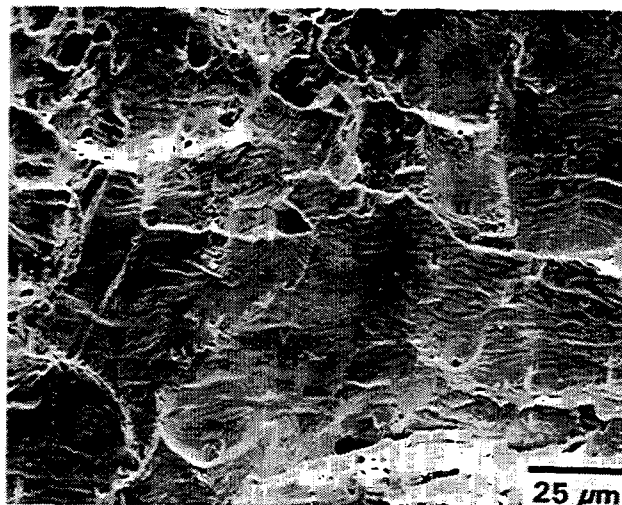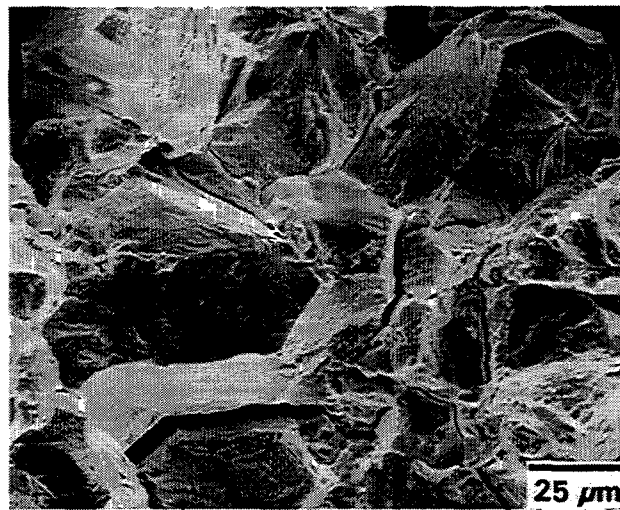Figure 3.   J-R curves for Alloy 690 Heat B in water.

Figure 4.   Effect of displacement rate on the cracking behavior of Alloy 690 Heat B in water.
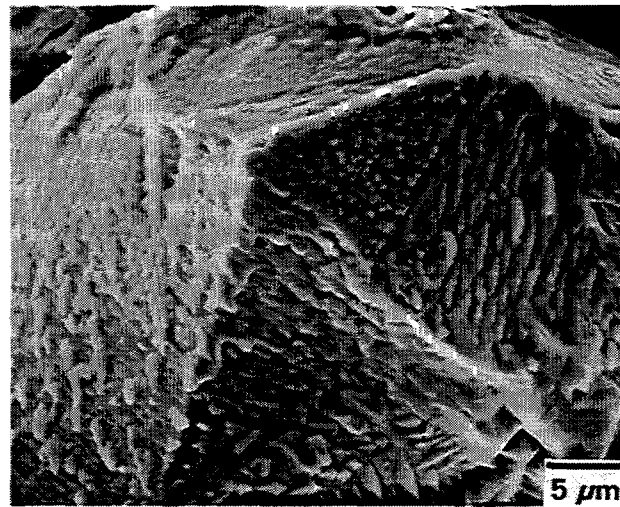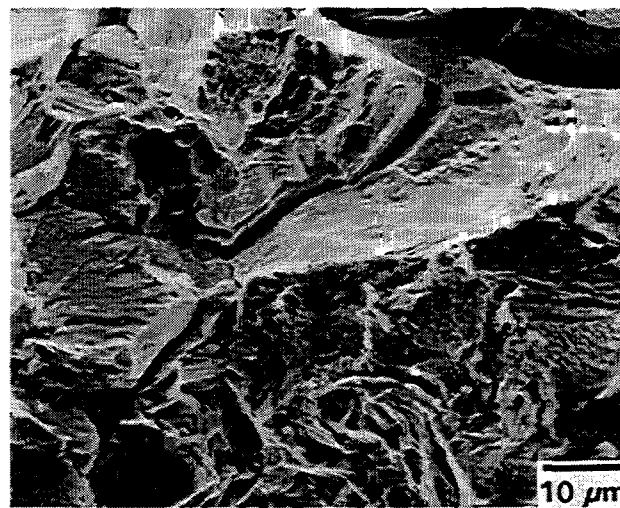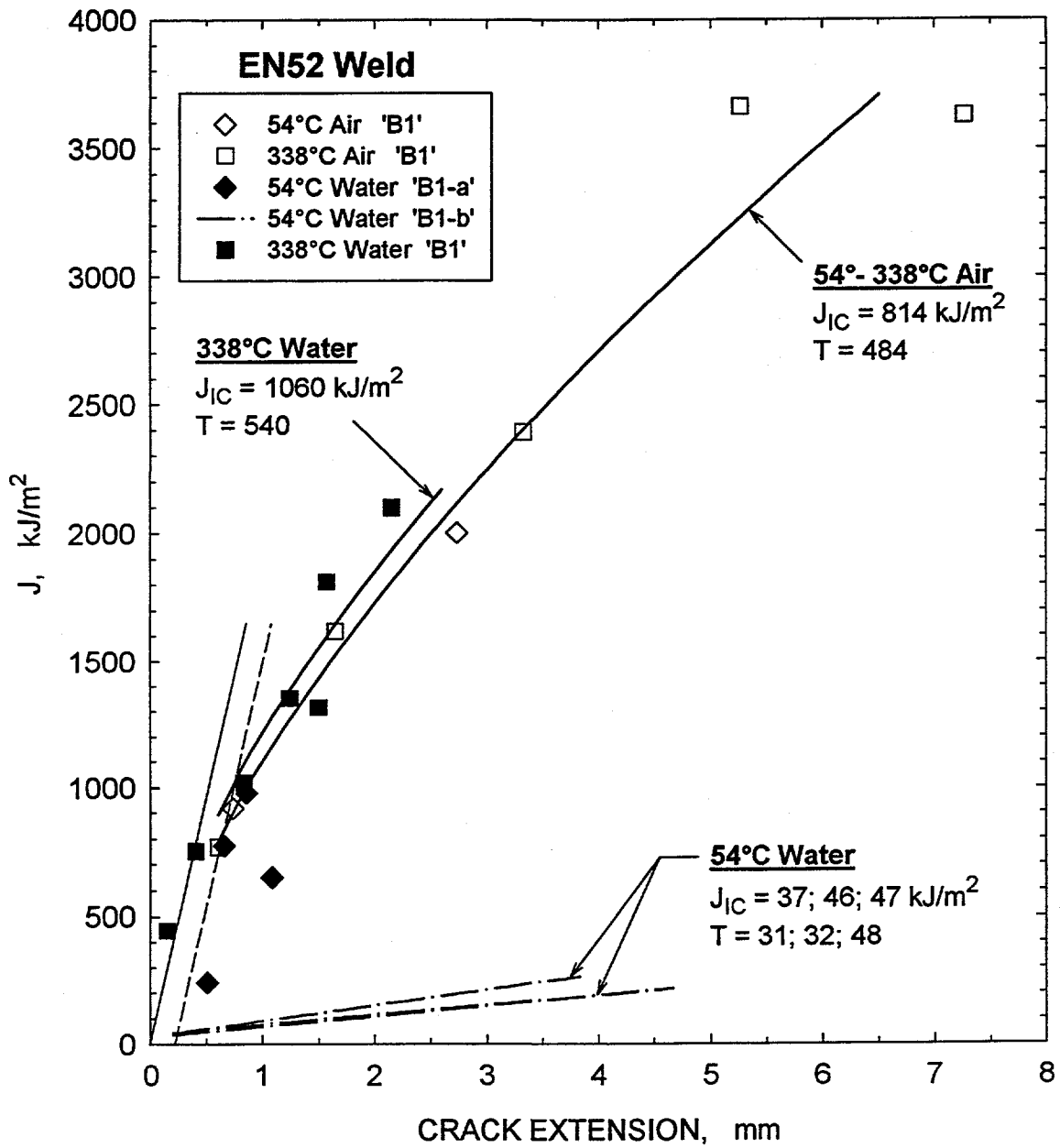
(a)

(b)

(c)

690FR1.cdr

Figure 5.   Fracture surface features for Alloy 690 tested in air and 338°C water were indistinguishable. (a) 338°C air. Duplex dimple morphology with large dimples nucleated by large carbide inclusions and smaller dimples nucleated by ghost boundary carbides. Note evidence of serpentine slip offsets and elongated shear dimples in the shear-stretch region (on right side). (b) 338°C water. Large and small dimples. (c) 338°C water. Typical shear-stretch region.

690FR2.cdr

Figure 6.   SEM fractographs of Alloy 690 tested in 54°C water showing intergranular cracking but no evidence of dimple rupture. (a) Intergranular cracking and poorly defined transgranular facets. (b) High magnification of upper right corner of (a) showing rough appearance of grain boundary walls. (c) Poorly defined transgranular facets.

Figure 7.   J-R curves for EN52 weld 'B1' in air and water.

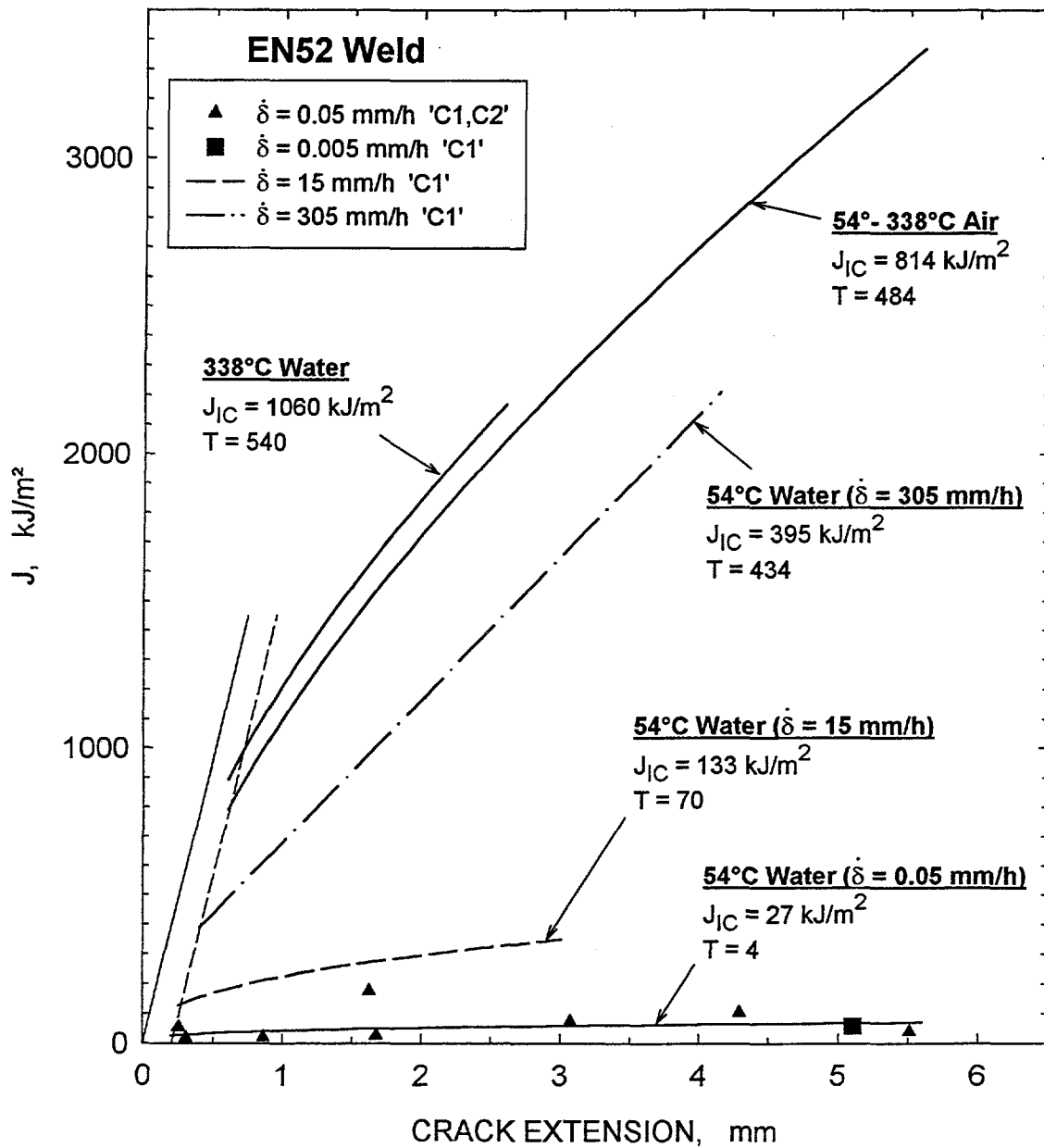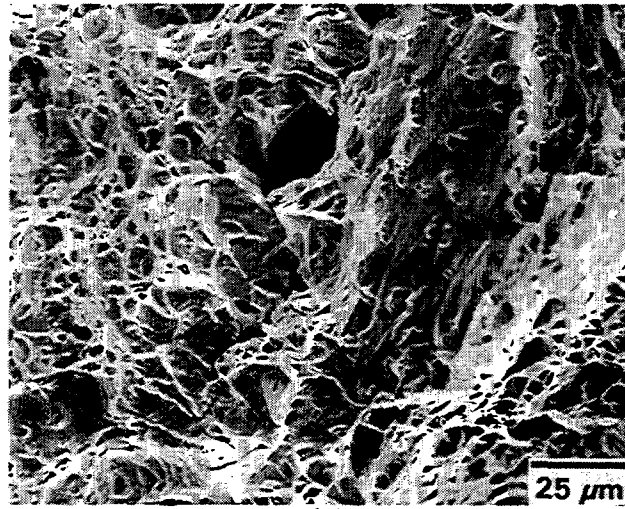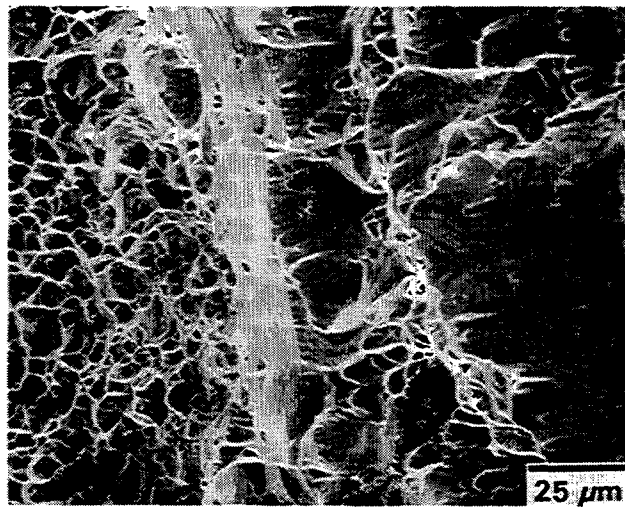Figure 8.   J-R curves for EN52 welds 'C1' and 'C2' in water.

EN52 Weld

▲ $\dot{\delta}$ = 0.05 mm/h 'C1,C2'
■ $\dot{\delta}$ = 0.005 mm/h 'C1'
— — $\dot{\delta}$ = 15 mm/h 'C1'
— ·· $\dot{\delta}$ = 305 mm/h 'C1'

54°- 338°C Air

J_{IC} = 814 kJ/m^2
T = 484

338°C Water

J_{IC} = 1060 kJ/m^2
T = 540

54°C Water ($\dot{\delta}$ = 305 mm/h)

J_{IC} = 395 kJ/m^2
T = 434

54°C Water ($\dot{\delta}$ = 15 mm/h)

J_{IC} = 133 kJ/m^2
T = 70

54°C Water ($\dot{\delta}$ = 0.05 mm/h)

J_{IC} = 27 kJ/m^2
T = 4

J, kJ/m^2

CRACK EXTENSION, mm

Figure 9.   Effect of displacement rate on the cracking behavior of EN52 welds 'C1' and 'C2'.

Figure 10. Fracture surface features for EN52 welds tested in air and 338°C water were indistinguishable. (a) 54°C air. Dimples and shear-stretch region (upper right). (b) 338°C water. Dimples (left) and shear-stretch region (right).

52FR2d.cdr

(a)

(b)

Figure 11.   SEM fractographs of EN52 welds tested in 54°C water. (a) Dominant intergranular cracking morphology surrounding island of transgranular faceting (bottom center). (b) Intergranular fracture surfaces were rather featureless.
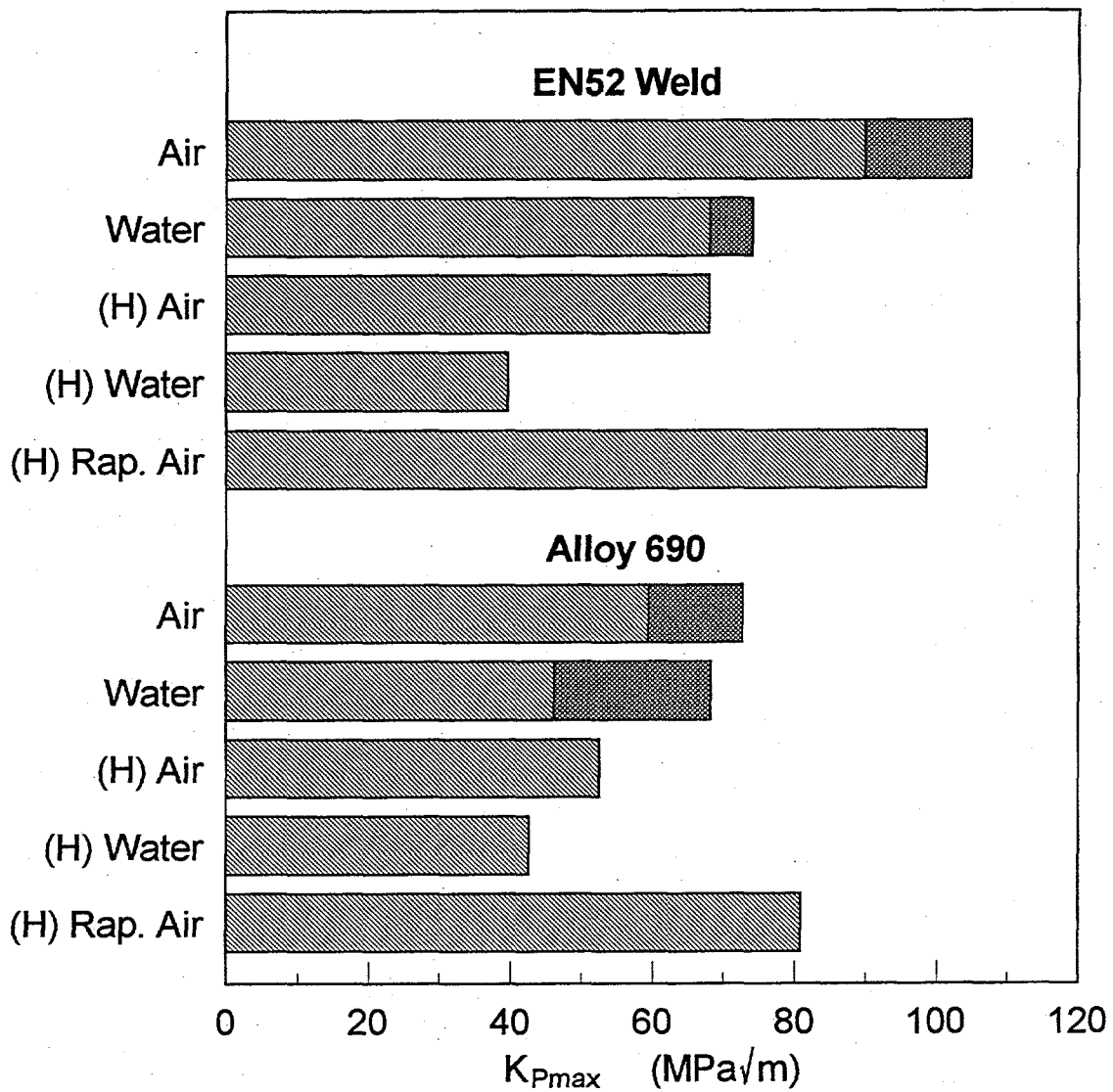
Figure 12. K_{Pmax} values for EN52 weld and Alloy 690. Non-precharged specimens were tested in 54°C air or water; hydrogen-precharged [H] specimens were tested in 24°C air or water. The short test times for the rapid loading tests [Rap], where maximum load was reached in 1 to 3 seconds, preclude hydrogen from diffusing to the crack tip, so bulk hydrogen levels control fracture behavior. Cross-hatching represents a range of K_{Pmax} values.
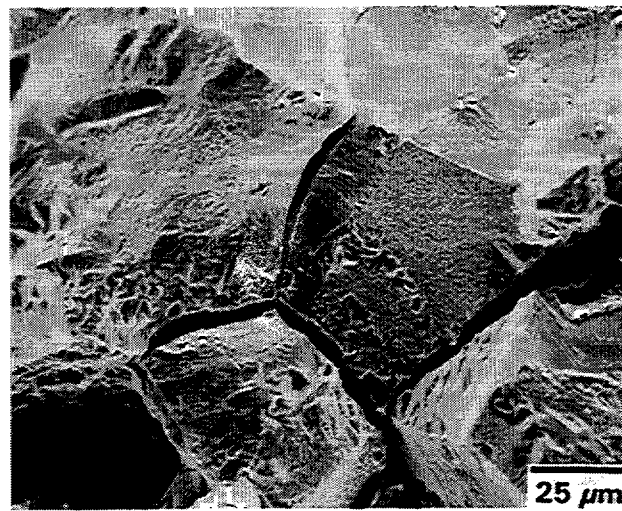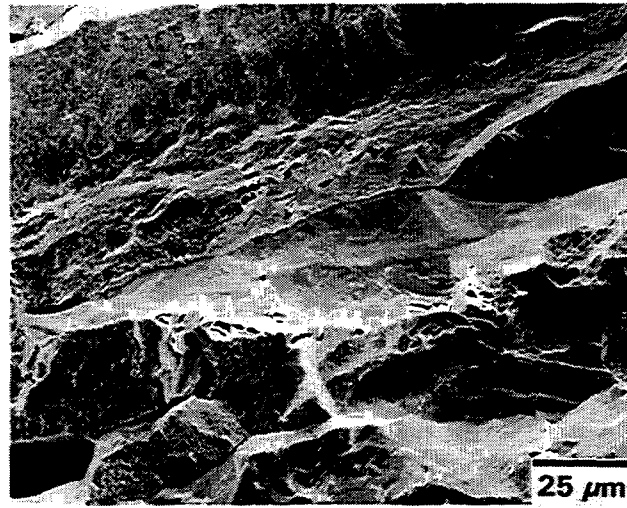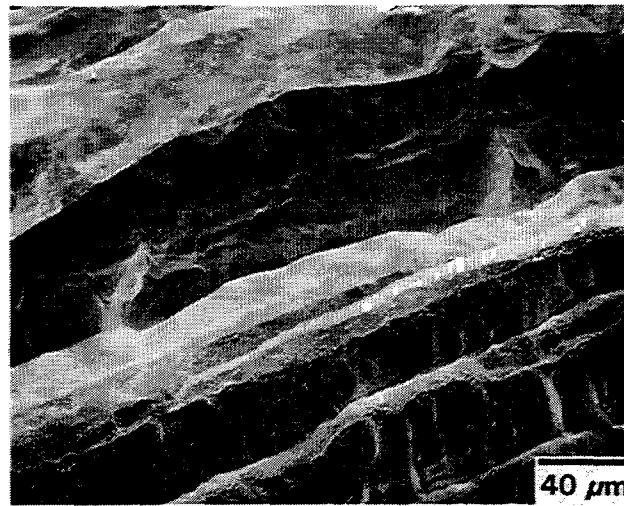
(a)
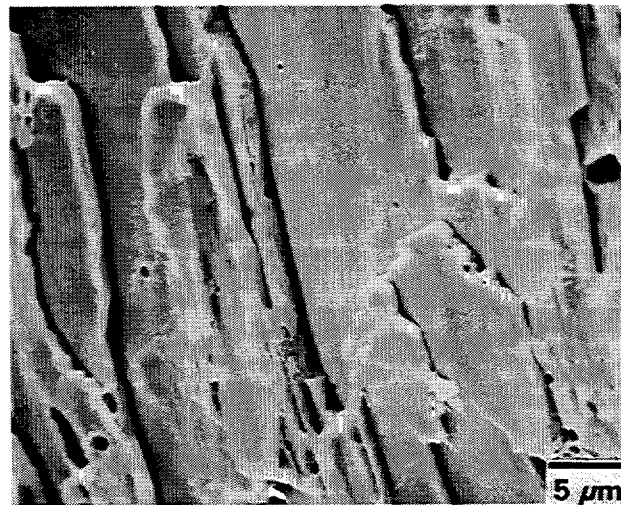
(b)
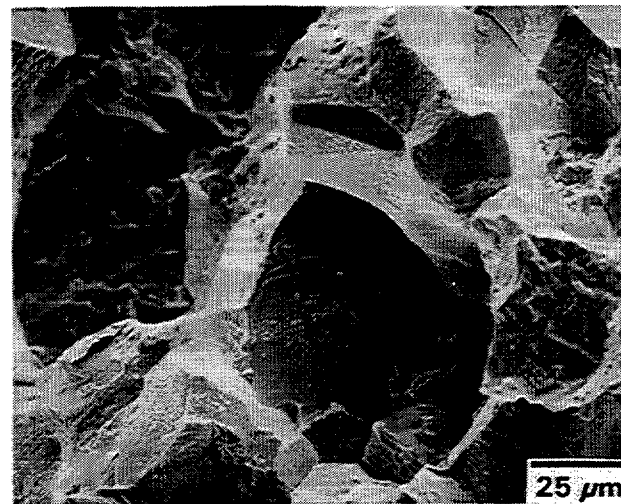
(c)

690FR3.cdr

Figure 13.   Fracture surface morphology for hydrogen-precharged Alloy 690. (a) Tested in air. Intergranular cracking and transgranular faceting. (b) Tested in air. Crystallographic facets steeply inclined to fracture surface.   (c) Tested in water. Intergranular cracking and transgranular faceting.

(a)

(b)

Figure 14. Fracture surface morphology for hydrogen-precharged EN52 welds. (a) Tested in air. Extensive intergranular cracking with small transgranular islands. (b) Tested in water. Fracture surface is predominantly intergranular.

52FR3d.cdr